Locations of the Hydrophobic Side Chains of Lipoglycopeptides Bound to the Peptidoglycan of *Staphylococcus aureus*

Sung Joon Kim,[†] Kelly S. E. Tanaka,[‡] Evelyne Dietrich,[‡] Adel Rafai Far,[‡] and Jacob Schaefer*,[#]

[†]Department of Chemistry and Biochemistry, Baylor University, Waco, Texas 76798, United States
[‡]The Medicines Company, Saint Laurent, Quebec H4S 2A1, Canada
[#]Department of Chemistry, Washington University, St. Louis, Missouri 63130, United States

Ⓢ *Supporting Information*

ABSTRACT: Glycopeptides whose aminosugars have been modified by attachment of hydrophobic side chains are frequently active against vancomycin-resistant microorganisms. We have compared the conformations of six such fluorinated glycopeptides (with side chains of varying length) complexed to cell walls labeled with D-[1-^{13}C]alanine, [1-^{13}C]glycine, and L-[ε-^{15}N]lysine in whole cells of *Staphylococcus aureus*. The internuclear distances from ^{19}F of the bound drug to the ^{13}C and ^{15}N labels of the peptidoglycan, and to the natural abundance ^{31}P of lipid membranes and teichoic acids, were determined by rotational-echo double resonance NMR. The drugs did not dimerize, and their side chains did not form membrane anchors but instead became essential parts of secondary binding to pentaglycyl bridge segments of the cell-wall peptidoglycan.
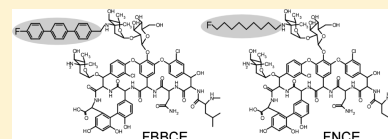
N-Alkylation of the vancosamine residue of a glycopeptide by a hydrophobic group significantly increases antimicrobial activity against a broad spectrum of Gram-positive microorganisms. While there is no conserved structure required for the drug side chain, chloroeremomycin (Supporting Information, Figure S1, top left) derivatives having a hydrophobic moiety with a length between 7 and 13 equivalent carbon units (ECU) all exhibit significant enhancements in activity relative to their parent compounds.[1,2] For example, alkylation of the disaccharide 4-epivancosamine of chloroeremomycin by a benzyl group results in *N*-(4-benzyl)chloroeremomycin (side-chain length of 5 ECU, Figure S1, top right) with a 2-fold enhancement in activity against vancomycin-resistant enterococci (VRE). An additional 32-fold enhancement is achieved by lengthening the side chain from 5 to 9 ECU in *N*-(4-(4-phenyl)benzyl)-chloroeremomycin (Figure S1, bottom left). However, further lengthening of the side chain to terphenyl in *N*-(4-(4-biphenyl)benzyl)-chloroeremomycin (Figure S1, bottom right) does not result in any enhancement in activity against VRE and diminishes activities against vancomycin-susceptible *Enterococcal faecium* and *Staphylococcus aureus* by factors of 4 and 16, respectively, relative to the activity of the parent compound, chloroeremomycin.[1,2]

Oritavancin (The Medicines Company, Parsippany, New Jersey, USA) (Figure S2, left) also has a side-chain length of 9 ECU.[3] Oritavancin was selected for clinical development because of its potent activity against a broad spectrum of Gram-positive bacteria including methicillin-resistant *S. aureus* (MRSA) and VRE. Oritavancin also has demonstrated activity against vancomycin-resistant *S. aureus* (VRSA) and VRE with minimum inhibitory concentrations (MICs) below 1 μg/mL.[4,5]

This side-chain-length dependent activity for disaccharide-modified glycopeptides is not limited to aryl-substitution.[1] In fact, an aliphatic side chain is found in second-generation glycopeptides including dalbavancin (Pfizer, USA) and telavancin (Theravance Inc., USA) whose chemical structures are shown in Figure S2. Dalbavancin is active against MRSA, vancomycin-intermediate resistant *S. aureus*, and VanB type VRE; dalbavancin is not active against VanA type VRE with MICs ≥ 32 μg/mL. Telavancin on the other hand presents some activity against all types of VRE (MIC of 8−16 μg/mL) and against VanA VRE and VRSA as well. Telavancin was approved by the FDA in 2009 for the treatment of complicated skin and skin-structure infections.
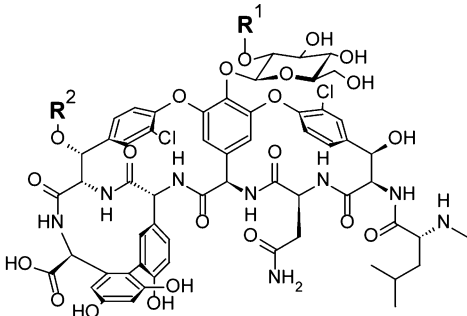
Because the sites of the hydrophobic side chains of oritavancin and telavancin are distant from the D-Ala-D-Ala-binding cleft of the aglycon structure (Figure S2), the improved antibacterial activities of these two drugs are unlikely to be the result of a direct interaction between side chains and the D-Ala-D-Ala termini of peptidoglycan structures like lipid II found in vancomycin-susceptible microorganisms, or the D-Ala-D-lactic-acid termini found in vancomycin-resistant microorganisms. The most widely accepted proposed mode of action for disaccharide modified glycopeptides is that the drug hydrophobic side chains mediate the formation of a drug dimer and act as a membrane anchor,[6] thereby resulting in improved binding to the lipid II target. Other possibilities are that the drug targets a specific membrane protein,[7,8] or that the anchoring induces membrane disruption, as shown by the loss of membrane potential and increase in membrane permeability.[9] However, *in situ* characterization of oritavancin binding in intact whole cells of *S. aureus* by solid-state NMR[10,11] has shown that the drug is a monomer bound to the peptidoglycan cell wall and makes no membrane contact. Membrane
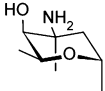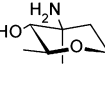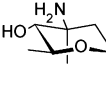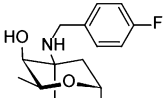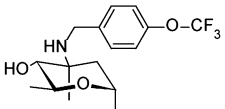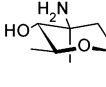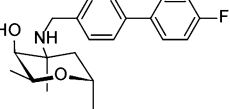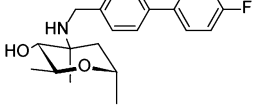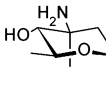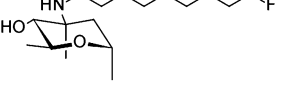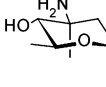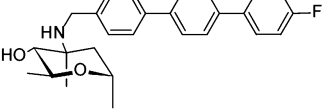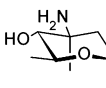
	R¹	R²	R¹ chain length
Vancomycin		H	0
Chloroeremomycin			0
FBV		H	5
LY309687			7
FPBV		H	9
[¹⁹F]oritavancin			9
FNCE			9
FBBCE			13

Figure 1. Chemical structures of fluorine-containing, disaccharide-modified glycopeptide antibiotics and their parent compounds. *N*-(4-Fluorobenzyl)vancomycin (FBV) is a vancomycin derivative with side-chain length of 5 equivalent carbon units (ECU). [¹⁹F]oritavancin is a chloroeremomycin derivative with side-chain length of 9 ECU. [¹⁹F]oritavancin differs from oritavancin by the substitution of F for Cl in the hydrophobic aryl side chain, which does not alter antimicrobial property. *N*-(4-(4-Fluorobiphenyl)benzyl)chloroeremomycin (FBBCE) has the longest side-chain length of 13 ECU. The side-chain length in *N*-(9-fluorononyl)chloroeremomycin (FNCE) is 9 ECU, identical to that of [¹⁹F]oritavancin. The fluorononyl side chain of FNCE is flexible, unlike the rigid fluorobiphenyl side chain of [¹⁹F]oritavancin. The chemical structure of FNCE closely resembles telavancin shown in Figure S2 (top right). Of all of these chemical compounds, [¹⁹F]oritavancin has the most potent antimicrobial activity. The MICs of [¹⁹F]oritavancin, FBBCE, and FNCE against *S. aureus* (ATCC 29213) are shown in Table S1.

interactions were observed only when oritavancin was complexed with isolated protoplast membranes of *S. aureus* in the absence of cell wall.[12] Furthermore, the proposed targeting of a specific membrane protein by the drug hydrophobic side chain is inconsistent with the observation of different effects on cell-wall biosynthesis by oritavancin in *S. aureus* and *E.*

faecium,[13] despite the similarities of the key membrane-associated enzymes in the two systems.

We have proposed before that oritavancin uses the cleft between its hydrophobic side chain and aglycon structure to target the pentaglycyl bridge of an uncross-linked stem, which can interfere with both transglycosylation and transpeptida-
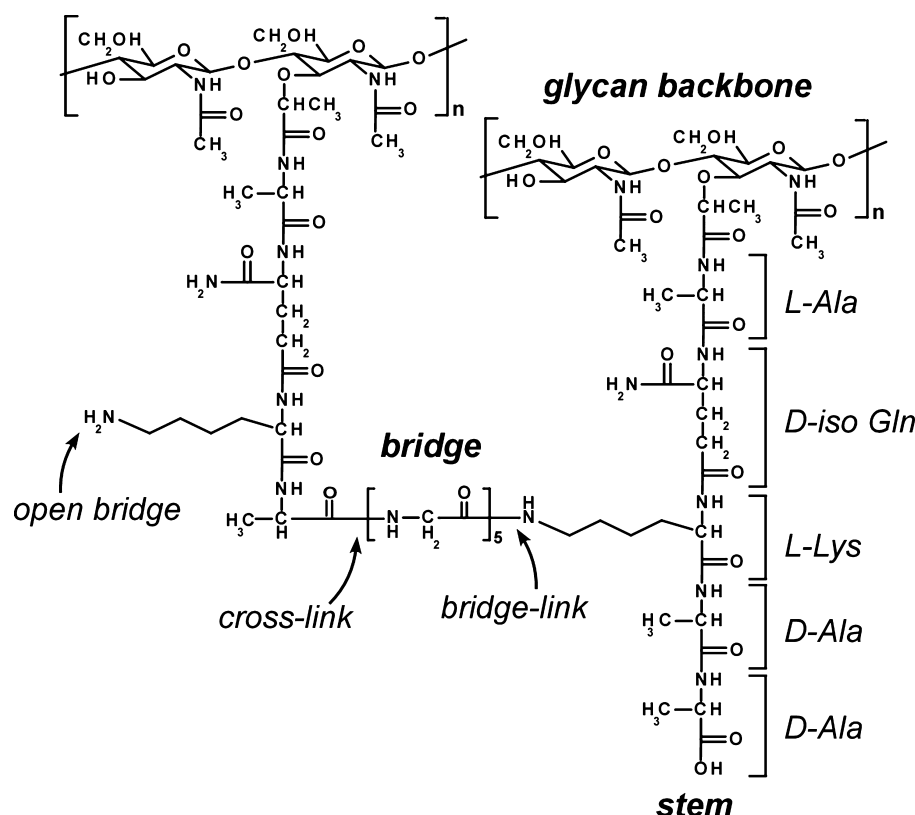
Figure 2. Chemical structure of *S. aureus* peptidoglycan. The uncross-linked peptidoglycan-stem structure consists of five amino acids, L-Ala, D-iso-Gln, L-Lys, D-Ala, and D-Ala. The peptidoglycan-bridge structure consists of five glycine residues in a compact helical conformation. The pentaglycyl bridging segment is attached to the ε-nitrogen of L-Lys of the peptidoglycan stem to form the bridge-link. The cross-link is a peptide bond between the C-terminus of the D-Ala of the fourth amino acid on one stem to the N-terminus of the pentaglycyl bridging segment of the adjacent peptidoglycan stem. The terminal D-Ala, the fifth amino acid of the peptidoglycan-stem, is cleaved upon formation of the cross-link.

tion[14] if the targeted stem is near the membrane surface. We formulated this proposal by comparing the cell wall-bound conformations of fluorinated disaccharide modified glycopeptides (Figure 1) *N*-(4-(fluorobenzyl)vancomycin (FBV), *N*-(4-(4-fluorophenyl)benzyl)vancomycin (FPBV), and [^{19}F]-oritavancin, complexed to the intact whole cells of *S. aureus*.[10,11,14] FBV has the shortest side chain with a length of 5 ECU, the minimum length required for any improvement in antibacterial activity.

In this report, we describe the effects of lengthening the hydrophobic side-chain length to greater than 9 ECU (Figure 1) on the secondary binding-site conformation by synthesizing FBBCE, which has a fluoroterphenyl side chain with a length of 13 ECU. In addition, we describe the effects of replacing the rigid biphenyl side-chain found in oritavancin by a flexible nonyl side chain with equal chain length of 9 ECU (Figure 1) by synthesizing FNCE. These two drugs were complexed to intact whole cells of *S. aureus* grown in defined media containing D-[1-^{13}C]alanine, or [1-^{13}C]glycine and L-[ε-^{15}N]-lysine, to label the cross-link, bridge-link, and pentaglycyl segment of cell-wall peptidoglycan (Figure 2). The conformations of FBBCE- and FNCE-peptidoglycan complexes were then characterized by determining the drug ^{19}F positions with respect to the cross-link, bridge-link, and pentaglycyl bridge using ^{13}C{^{19}F} and ^{15}N{^{19}F} rotational-echo double resonance (REDOR) NMR.[15]

■ MATERIALS AND METHODS

Synthesis of FBBCE and FNCE. The detailed chemical syntheses of FBBCE and FNCE (Figure S3) are presented in the Supporting Information.

Susceptibility Testing. Minimum inhibitory concentrations for [^{19}F]oritavancin, FBBCE, and FNCE against *S. aureus* (ATCC 29213) were determined using the broth microdilution method without polysorbate 80, as was formerly recommended for oritavancin by the National Committee for Clinical Laboratory Standards (Table S1).

Complexes of Semisynthetic Glycopeptides to Whole Cells of *S. aureus*. Glycopeptides were complexed to *S. aureus* that had been harvested at the end of exponential growth to yield drug-bound whole-cell complexes. The detailed protocols for the defined medium, *S. aureus* standard medium (SASM), and for growing *S. aureus* (ATCC 6538P) are described elsewhere.[10,11,16] For FBCCE complexed to the whole cells, 4.1 mg of FBBCE (2.5 μmol) was dissolved in 15 mL of 40 mM triethanolamine buffer, which was used to resuspend harvested whole cell of *S. aureus* grown in 400 mL of SASM. In one sample, the SASM contained D-[1-^{13}C]alanine and alanine racemase inhibitor alaphosphin (5 μg/mL). In the other sample, the SASM contained [1-^{13}C]glycine and L-[ε-^{15}N]-lysine. On the basis of a vancomycin-binding assay,[10] the estimated FBBCE binding-site occupancy for both samples was 32%. For FNCE complexed to the whole cells, 4.0 mg of FNCE (2.2 μmol) was dissolved in 15 mL of 40 mM triethanolamine buffer, which was used to resuspend harvested whole cells of *S. aureus* grown in 400 mL of SASM. In one sample, SASM
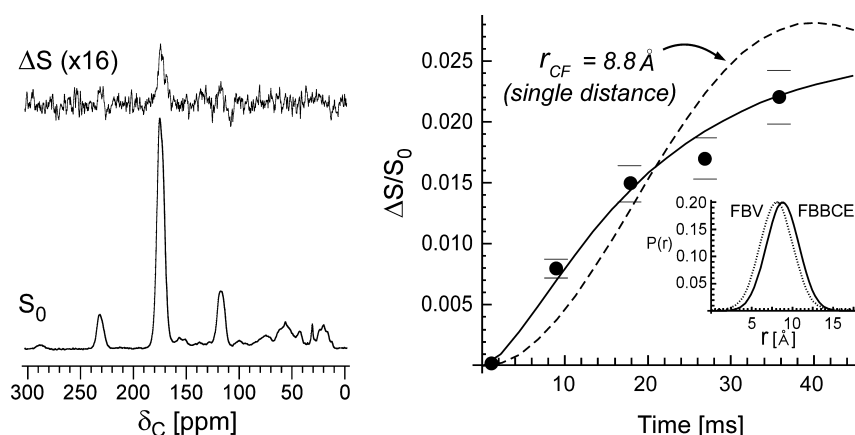
Figure 3. (Left) 125-MHz $^{13}C\{^{19}F\}$ REDOR spectra of a FBBCE complex of whole cells of *S. aureus* labeled by D-[1-^{13}C]alanine in the presence of an alanine racemase inhibitor after dipolar evolution of 17.9 ms. The spectra are the result of the accumulation of 104 488 scans at a 12-T static magnetic field with MAS at 7143 Hz. The full-echo (S_0) spectrum is at the bottom of the figure and the REDOR difference spectrum (ΔS) is shown at the top. (Right) REDOR dephasing ($\Delta S/S_0$) for the 175-ppm peak. The calculated $^{13}C\{^{19}F\}$ REDOR dephasing for a $^{13}C-^{19}F$ distance of 8.8 Å without a distribution is represented by the dashed line, and with a distribution by the solid line. A broad $^{13}C-^{19}F$ distance distribution for the FBBCE−peptidoglycan complex (inset, solid line) indicates conformational heterogeneity. Similar conformational heterogeneity was observed (see ref 14) for the FBV−peptidoglycan complex whose $^{13}C-^{19}F$ distance distribution is shown as the dotted line in the inset.
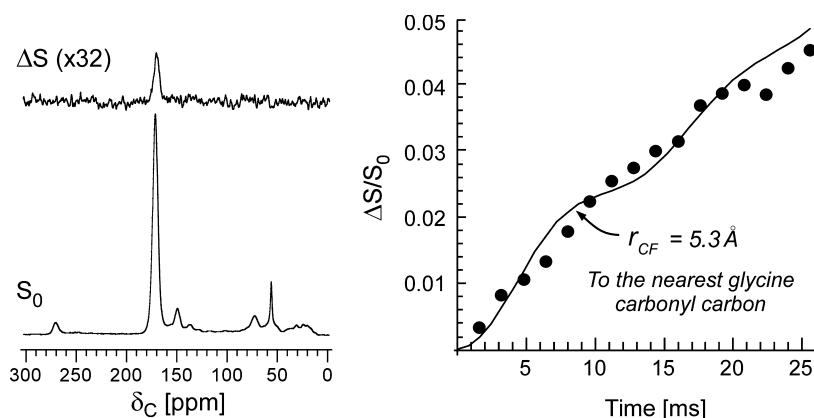

Figure 4. (Left) 50.3-MHz $^{13}C\{^{19}F\}$ REDOR spectra of a FBBCE complex of whole cells of *S. aureus* labeled by [1-^{13}C]glycine after dipolar evolution of 6.4 ms. The spectra are the result of the accumulation of 10 000 scans at a 4.7-T static magnetic field with MAS at 5000 Hz. The full-echo (S_0) spectrum is at the bottom of the figure and the REDOR difference spectrum (ΔS) is shown at the top. (Right) REDOR dephasing ($\Delta S/S_0$) for the 171-ppm peak. The solid line is the calculated dephasing for the best fluorine position in FBBCE−peptidoglycan complex shown in Figure 5 (bottom right). Error bars (based on signal-to-noise of ΔS) are contained within the width of the solid-circle symbols.

contained D-[1-^{13}C]alanine and alanine racemase inhibitor alaphosphin (5 μg/mL), and the second sample contained [1-^{13}C]glycine and L-[ε-^{15}N]lysine. The estimated FNCE binding-site occupancy for both samples was 29%, not significantly different from that for FBBCE. The bacteria-glycopeptide mixture was equilibrated on ice for 5 min prior to freezing followed by lyophilization.

Dipolar Recoupling. Rotational-echo double resonance (REDOR), a solid-state NMR method that recouples dipolar interactions under magic-angle spinning,[15] was used to determine heteronuclear dipolar couplings and hence internuclear distances. A brief description of REDOR is presented in the Supporting Information. Details of the REDOR pulse sequence are presented at the end of the next section.

Solid-State NMR Spectrometers and Pulse Sequences. REDOR was performed at two different static magnetic fields, at 12-T (proton radio frequency of 500 MHz) and at 4.7-T (proton radio frequency of 200 MHz). The $^{13}C\{^{19}F\}$ and $^{15}N\{^{19}F\}$ REDOR results of Figures 3 and 6 (middle) were performed at 12-T provided by an 89-mm bore Magnex

(Oxfordshire, England) superconducting solenoid. REDOR was performed using a six-frequency transmission-line probe having a 12-mm long, 6-mm inner diameter analytical coil and a Chemagnetics/Varian ceramic spinning module. The lyophilized whole-cell sample was contained in a thin-wall Chemagnetics/Varian (Fort Collins, CO/Palo Alto, CA) 5-mm outer diameter zirconia rotor and spun at 7143 Hz with the speed under active control within ±2 Hz. A Tecmag Libra pulse programmer (Houston, TX) controlled the spectrometer. Two-kW American Microwave Technology power amplifiers were used to produce radio frequency pulses for ^{13}C (125 MHz) and ^{15}N (50.3 MHz). The ^{1}H (500 MHz) and ^{19}F (470 MHz) radio frequency pulses were generated by 2-kW Creative Electronics tube amplifiers driven by 50-W American Microwave Technology power amplifiers. The π pulse lengths were 8 μs for ^{13}C and ^{15}N, and 5 μs for ^{19}F. Proton-carbon matched cross-polarization transfers were made in 2 ms at 62.5 kHz. Proton dipolar decoupling was 100 kHz during data acquisition, and TPPM of the ^{1}H radio frequency[17] was used throughout both dipolar evolution and decoupling periods.
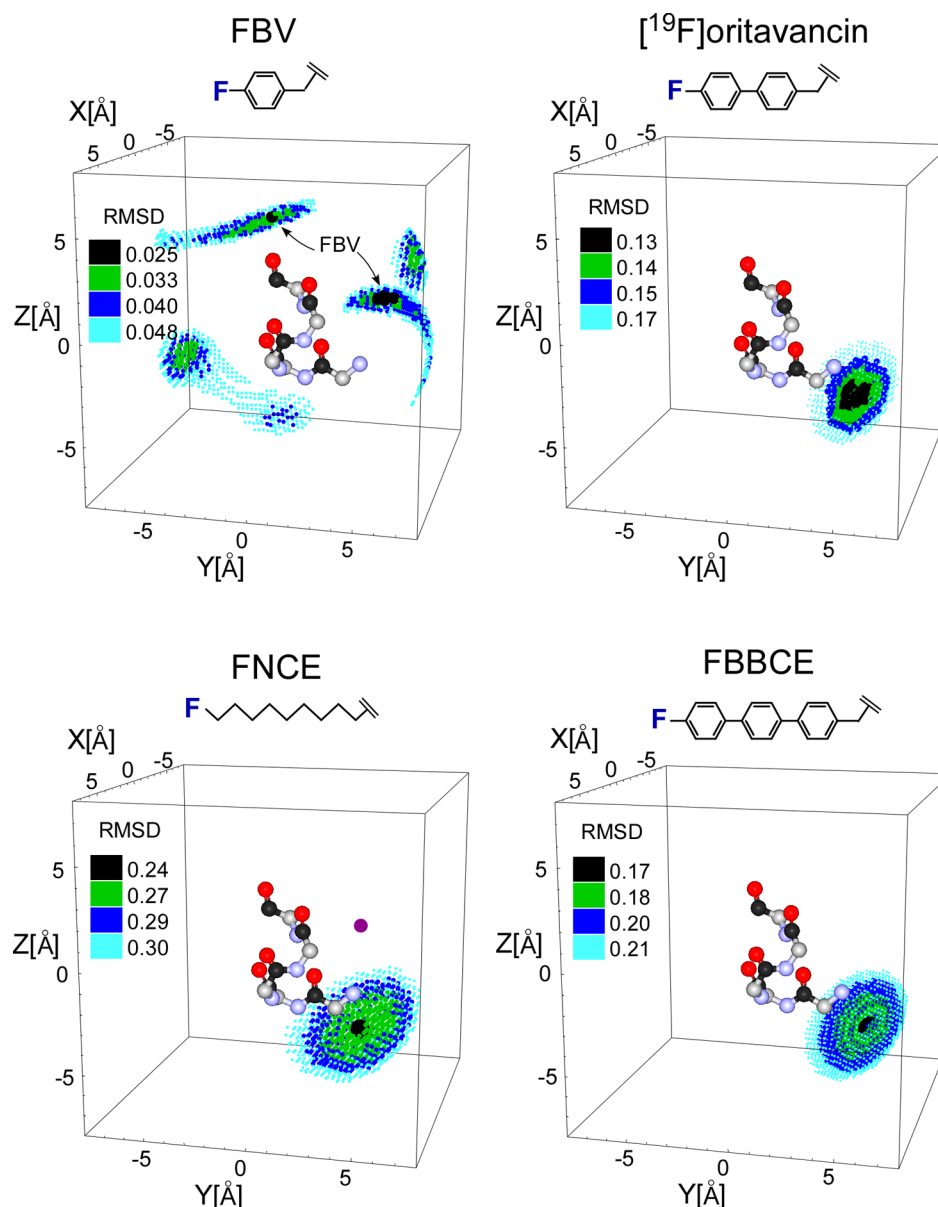
Figure 5. Possible positions of fluorine relative to the bridging pentaglycyl helix in peptidoglycan complexes of FBV (top left), [^{19}F]oritavancin (top, right), FNCE (bottom, left), and FBBCE (top right). The pentaglycyl bridge is shown in an α-helical conformation with carbonyl carbons in black, alpha carbons in gray, nitrogens in blue, and oxygens in red. The positions that are consistent with the ^{13}C{^{19}F} REDOR dephasing are indicated by small spheres whose colors indicate the root-mean-square deviation between calculated and experimental dephasing. The best position of the fluorine of FBV, with side-chain length of 5 ECU, when bound to the peptidoglycan is at the middle of the pentaglycyl helix bridge structure. In contrast, the fluorine positions of [^{19}F]oritavancin, FNCE, and FBBCE are found at the end of the helix near the cross-link. Despite the flexibility in the fluorononyl side chain, the fluorine positions of FNCE are also restricted to the end of the helix near the cross-link, far from the middle of the bridge (purple dot).

The ^{13}C{^{19}F} and ^{15}N{^{19}F} REDOR results of Figure 4, Figure 6 (left and right), and Figure 7 were performed at 4.7-T static magnetic field (proton radio frequency of 200 MHz) provided by an 89-mm bore Oxford (Cambridge, England) superconducting solenoid. REDOR was performed using a 4-frequency transmission-line probe with a 17-mm long, 8.6-mm inside-diameter analytical coil and a Chemagnetics/Varian ceramic stator. Lyophilized whole-cell samples were contained in Chemagnetics/Varian 7.5-mm outside-diameter zirconia rotors. The rotors were spun at 5000 Hz with the speed under active control to within ±2 Hz. A Tecmag Libra pulse programmer controlled the spectrometer. The ^{1}H (200 MHz) radio frequency pulses were produced by a 1-kW Kalmus

Engineering Int. Ltd. (Valencia, CA) power amplifier, and the ^{19}F (188 MHz) pulses by a 1-kW Dressler Hochfrequenztechnik Gmbh (Stolberg-Vicht, Germany) power amplifier. Radio frequency pulses for ^{13}C (50.3 MHz) and ^{15}N (20.3 MHz) were produced by 1-kW ENI (Andover, MA) LPI-10 power amplifiers. The π-pulse lengths were 10 μs for ^{19}F, ^{13}C, and ^{15}N. Proton-carbon matched cross-polarization transfers were made in 2 ms at 50 kHz. The single-frequency proton dipolar decoupling was 98 kHz throughout dipolar evolution and data acquisition.

To eliminate long-term drifts in the performance of the spectrometers due to component aging and minor changes in the temperature of the room, spinning gas, and the amplifiers,

all power amplifiers for each radio frequency for both spectrometers were under active control.[18] The S and S_0 alternate-scan strategy compensated for short-term drifts. Standard XY-8 phase cycling[19] was used for all observed-channel refocusing π pulses (at the end of each rotor period during dipolar evolution) and dephasing pulses (at the half rotor periods) to compensate for pulse imperfections.[20] The recycle delay period was 2 s during which each amplifier produced a 300-μs test pulse. The diode detected voltages were compared to a reference voltage previously calibrated. The resulting differences were used to correct the drives of the power amplifiers for the next repetition of the REDOR pulse sequence. Combination of the active control of the amplifiers and the alternate-scan data acquisition for each pair of REDOR spectra (S and S_0) eliminated long-term drifts in the performance of the spectrometer.[18] Data accumulation times of weeks were practical. The spectra of Figure 3, for example, each took 5 days to accumulate (3 weeks for the $\Delta S/S_0$ plot), while those of Figure 4 each took a half day (1 week for the $\Delta S/S_0$ plot).

Calculated REDOR Dephasing. REDOR dephasing was calculated using the modified Bessel function expressions given by Mueller et al.[21] and de la Caillerie and Fretigny[22] for a spin-$\frac{1}{2}$ pair. For ^{19}F of glycopeptide coupling to D-[1-^{13}C]Ala, the parameters (mean and width) describing the ^{19}F–^{13}C distance distribution were allowed to vary to minimize the root-mean-square deviation (rmsd) between the experimental and calculated dephasing.[10,23] For all possible ^{19}F positions of glycopeptides relative to a model pentaglycyl bridge, the rmsd values were calculated for coordinate space at 0.2 Å resolution using an error function.[14]

■ RESULTS

^{13}C{^{19}F} REDOR of FBBCE Complexed to *S. aureus* Labeled by D-[1-^{13}C]Ala. ^{13}C{^{19}F} REDOR spectra during 17.9 ms dipolar evolution are shown in Figure 3 (left), with the 175-ppm dephasing ($\Delta S/S_0$) as a function of dipolar evolution in Figure 3 (right). The calculated ^{13}C{^{19}F} REDOR dephasing for a single distance of 8.8 Å (dashed line) does not match the experiment. (The maximum D-[1-^{13}C]alanine dephasing limit of 3% was calculated as described in detail for the FNCE complex in a later section.) A better match was obtained by the calculated dephasing for ^{13}C–^{19}F distances centered at 8.8 Å (Figure 3, right, solid line) and the distribution shown in the figure inset. The broad ^{13}C–^{19}F distance distribution is consistent with conformational heterogeneity in the FBBCE–peptidoglycan complex. A similar ^{13}C–^{19}F distance distribution (centered at 7.8 Å) has been also observed for the FBV–peptidoglycan complex (Figure 3, right, inset, dotted line).[14] For [^{19}F]oritavancin- and FPBV-peptidoglycan complexes, however, single ^{13}C–^{19}F distances without distributions were observed.[10,11]

^{13}C{^{19}F} REDOR of FBBCE Complexed to *S. aureus* Labeled by [1-^{13}C]Gly. ^{13}C{^{19}F} REDOR spectra during 6.4 ms dipolar evolution are shown in Figure 4 (left), with the 171-ppm glycyl-carbonyl carbon $\Delta S/S_0$ as a function of dipolar evolution, in Figure 4 (right, solid circles). The calculated dephasing (solid line) was done assuming the best-fit ^{19}F positions of FBBCE relative to the five carbonyl carbons of the pentaglycyl bridging segment in the compact helical conformation shown in Figure 5 (bottom right, black spheres). The dephasing limit of 7.4% in Figure 4 was estimated based on the product of the binding-site occupancy of 32% (see above), the

fraction of peptidoglycan stem structures terminating in D-Ala-D-Ala of 46%[24] for *S. aureus* (ATCC 6538P), and a fractional cell-wall contribution to the 171-ppm peak in the S_0 spectrum of 50%.[10,11]

The possible ^{19}F positions for the FBBCE-peptidoglycan complex shown in Figure 5 are clustered around the cross-link terminus of the pentaglycyl helical bridge. The distances between the best ^{19}F position of FBBCE (black circle) to the glycyl-carbonyl carbons of the pentaglycyl bridge, starting from the cross-linked Gly$_5$ to the bridge-linked Gly$_1$, are 5.3, 8.0, 9.7, 9.8, and 11.2 Å, respectively. The best ^{19}F position of FBBCE–peptidoglycan complex is nearly superimposable with the best ^{19}F position found in the [^{19}F]oritavancin–peptidoglycan complex.[10] In the latter, the distances from the ^{19}F of [^{19}F]oritavancin to Gly$_5$ through Gly$_1$ were 5.0, 7.6, 9.4, 9.6, and 10.9 Å, respectively. Lengthening of the side chain from biphenyl in [^{19}F]oritavancin to terphenyl in FBBCE did not significantly change the fluorine position with respect to the pentaglycyl bridge.

^{15}N{^{19}F} REDOR of FBBCE Complexed to *S. aureus* Labeled by L-[ε-^{15}N]Lys. ^{15}N{^{19}F} REDOR spectra after 22.4 ms of dipolar evolution are shown in Figure 6 (right). The ^{15}N-lysyl amide peak at 95 ppm is unique to the bridge link of the peptidoglycan. The absence of lysyl amide-peak dephasing in the difference spectrum positions the ^{19}F in FBBCE–peptidoglycan more than 9 Å from the bridge-link (Figure 5, bottom right). The ^{19}F position for the [^{19}F]oritavancin complex (Figure 5, top right) is also more than 9 Å from the
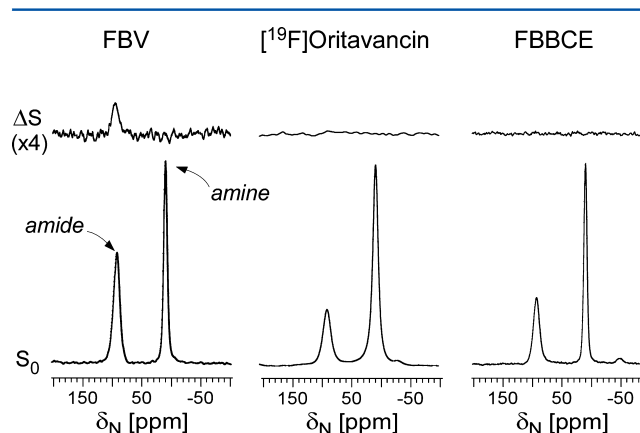

Figure 6. ^{15}N{^{19}F} REDOR spectra of whole cells of *S. aureus* grown in defined medium containing L-[ε-^{15}N]lysine complexed with glycopeptides with varying aryl-side-chain lengths. The full-echo spectra are at the bottom of the figure and the corresponding difference spectra at the top. (Left) For the FBV–peptidoglycan complex, the ^{15}N-lysl-amide peak at 95 ppm is dephased by the fluorine after 19.2 ms of dipolar evolution. This positions the fluorine on FBV approximately 7.0 Å from the bridge link of L-[ε-^{15}N]lysine at the middle of the pentaglycyl helix. The spectra are the result of the accumulation of 80 000 scans at a 4.7-T static magnetic field with MAS at 5000 Hz. (Middle) For the [^{19}F]oritavancin-peptidoglycan complex, the absence of dephasing after 17.9 ms of dipolar evolution positions the fluorine of [^{19}F]oritavancin more than 9.0 Å from the L-[ε-^{15}N]lysine of the bridge link. The spectra are result of the accumulation of 100 000 scans at a 12-T static magnetic field with MAS at 7143 Hz. (Right) For the FBBCE–peptidoglycan complex, no dephasing was observed even after 22.4 ms of dipolar evolution, consistent with the drug fluorine near the cross-link and distant from the bridge-link. The spectra are the result of the accumulation of 218 436 scans at a 12-T static magnetic field with MAS at 7143 Hz.
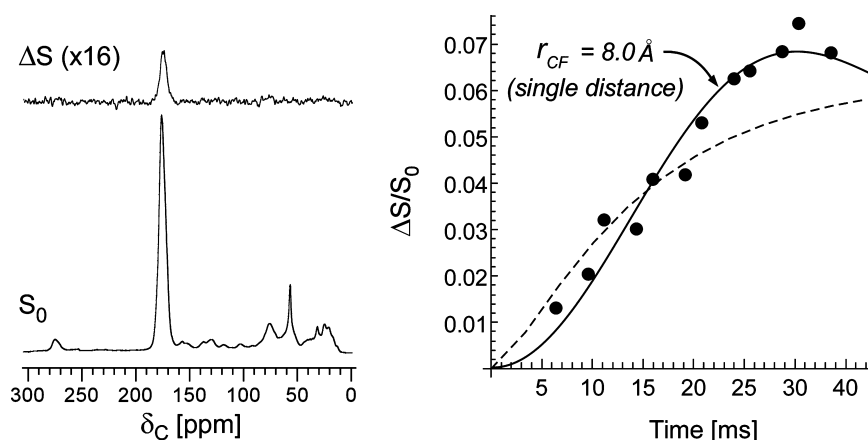
Figure 7. (Left) 50.3-MHz $^{13}C\{^{19}F\}$ REDOR spectra of the FNCE complex of whole cells of *S. aureus* labeled by D-[1-^{13}C]alanine in the presence of an alanine racemase inhibitor after dipolar evolution of 6.4 ms. The full-echo (S_0) spectrum is at the bottom of the figure and the REDOR difference spectrum (ΔS) is shown at the top. The spectra are the result of the accumulation of 40 000 scans at a 4.7-T static magnetic field with MAS at 5000 Hz. (Right) REDOR dephasing ($\Delta S/S_0$) for the 175-ppm peak. The solid line is the calculated $^{13}C\{^{19}F\}$ REDOR dephasing for a $^{13}C-^{19}F$ distance of 8.0 Å without a distance distribution, and the dashed line is for 8.0 Å with the same distribution shown in Figure 3 (inset, right) for FBBCE. Error bars (based on signal-to-noise of ΔS) are contained within the width of the solid-circle symbols.
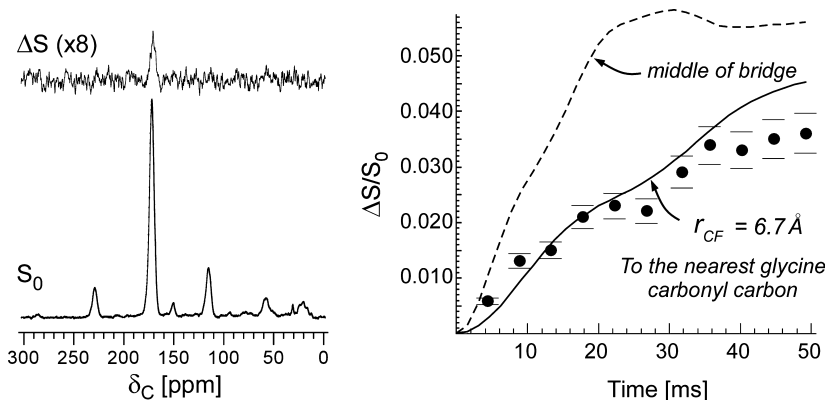

Figure 8. (Left) 125-MHz $^{13}C\{^{19}F\}$ REDOR spectra of the FNCE complex of whole cells of *S. aureus* labeled by [1-^{13}C]glycine after dipolar evolution of 17.9 ms. The spectra are result of the accumulation of 26 616 scans at 12-T static magnetic field with MAS at 7143 Hz. The full-echo (S_0) spectrum is at the bottom of the figure and the REDOR difference spectrum (ΔS) is shown at the top. (Right) REDOR dephasing ($\Delta S/S_0$) for the 171-ppm peak. The solid line is the calculated dephasing for the best fluorine position in FNCE-peptidoglycan complex shown in Figure 5 (bottom left). The dotted line is the calculated dephasing for the fluorine of FNCE positioned at the middle of the pentaglycyl bridge structure, as shown in Figure 5 (bottom left) by a purple dot.

bridge-link, whereas that for the FBV complex (Figure 5, top left), which shows REDOR dephasing (Figure 6, left), is approximately 7 Å from the bridge link.[14]

$^{13}C\{^{19}F\}$ REDOR of FNCE Complexed to *S. aureus* Labeled by D-[1-^{13}C]Ala. $^{13}C\{^{19}F\}$ REDOR spectra after dipolar evolution of 6.4 ms are shown in Figure 7 (left), with the 175-ppm dephasing (solid circles) as a function of dipolar evolution in Figure 7 (right). The maximum dephasing limit for FNCE complexed to whole cells labeled by D-[1-^{13}C]Ala was calculated based on the drug D-Ala-D-Ala primary binding-site occupancy (29%) times the fraction of peptidoglycan stems with a D-Ala-D-Ala terminus (46%) divided by the full echo contributions from (i) D-[1-^{13}C]alanine of cross-linked stems (54%), (ii) uncross-linked stems (46%), and (iii) D-[1-^{13}C]-alanine in teichoic acid which varies from 1.0 to 2.0 times the amount in cross-linked stems depending on growth conditions and assumed here to be 1.1.[24] Thus, the estimated asymptotical dephasing limit is $[\Delta S/S_0]_{limit}$ = (0.29)(0.46)/[(0.54)(1) + (0.46)(2) + (0.54)(1.1)] = 6.5%, which is in agreement with the observed dephasing limit of 6.5% (Figure 7, right). The

solid line is the calculated $^{13}C\{^{19}F\}$ REDOR dephasing curve for a single distance of 8.0 Å. The dashed line is the calculated dephasing curve for the distance of 8.0 Å with a broad distance distribution identical to that found for FBBCE−peptidoglycan complex (Figure 3, right, inset).

$^{13}C\{^{19}F\}$ REDOR of FNCE Complexed to *S. aureus* Labeled by [1-^{13}C]Gly. $^{13}C\{^{19}F\}$ REDOR spectra after dipolar evolution of 17.9 ms are shown in Figure 8 (left), with the dephasing of the glycyl carbonyl-carbon peak at 171 ppm plotted as a function of dipolar evolution (right, solid circles). The $^{13}C\{^{19}F\}$ dephasing (Figure 8, solid line) was calculated for the best-fit ^{19}F position of FNCE relative to the positions of the five carbonyl carbons of the pentaglycyl bridging segment, assuming the compact helical conformation shown in Figure 5 (bottom left, black spheres). A maximum dephasing limit of 6.0% was assumed. This value is in agreement with the estimated maximum dephasing limit of 6.6%, determined as the product of the binding-site occupancy (28%), the fraction of peptidoglycan stem structures terminat-

ing in D-Ala-D-Ala (46%), and the fraction of cell-wall contribution to the 171-ppm peak in the S_0 spectrum (50%).

The best-fit ^{19}F position for the FNCE−peptidoglycan complex is found near the cross-link terminus of the pentaglycyl helix bridge. Positioning the ^{19}F at the middle of the helix bridge (Figure 5, bottom left, purple dot) changes the calculated REDOR dephasing to values (Figure 8, right, dotted line), in poor agreement with the measured dephasing. The distances between the best-fit ^{19}F position of FNCE (black circle) to the glycyl-carbonyl carbon positions of the pentaglycyl bridge, starting from the cross-linked Gly_5 to the bridge-linked Gly_1 are 6.7, 9.1, 11.1, 11.5, and 12.6 Å, respectively. The ^{19}F positions of FNCE and [^{19}F]oritavancin are not superimposable (Figure 5).

^{31}P{^{19}F} REDOR. Figure S4 shows the ^{31}P{^{19}F} REDOR spectra after 13.4 ms of dipolar evolution for the FNCE complex (left) and the [^{19}F]oritavancin complex (right). The ^{31}P{^{19}F} detection range ($\Delta S/S_0 < 2\%$, or two times the noise level) is about 13 Å for these experiments, a distance greater than the lengths of the 9-carbon hydrophobic side chains. The detection-range estimate assumes that only 20% of S_0 is due to bilayer phosphorus in whole cells.[10] The fluidity of bilayers in lyophilized whole cells at room temperature is equivalent to that of fully hydrated bilayers at −38 °C in which head-to-tail ^{31}P−^{19}F dipolar coupling is readily detected.[25] The absence of dephasing for the FNCE complex (Figure S4, left) indicates that the ^{19}F of the drug side chain is not dipolar coupled to the natural-abundance ^{31}P of the lipid head groups. The possible minor dephasing for the oritavancin complex (Figure S4, top right) is consistent with that observed by Kim et al.[10] and is attributed to weak ^{31}P−^{19}F dipolar coupling between the drug's fluorine label and distant bilayer or lipoteichoic acid phosphates. Similar coupling to wall teichoic acid is not observed in isolated cell walls.[10] For both complexes, we conclude that the hydrophobic side chains are not embedded within the membrane. This conclusion is consistent with the absence of lipid natural-abundance ^{13}C aliphatic-carbon ^{13}C-{^{19}F} dephasing (Figures 7 and 8), which would have been expected from an embedded fluorine-labeled side chain and which is observed for [^{19}F]oritavancin complexed to cell-wall-free protoplast membranes.[12]

■ DISCUSSION

Membrane Anchors. The hydrophobic side chain is a prevalent motif found in numerous antibiotics including oritavancin, telavancin, ramoplanin, amphomycin, daptomycin, plusbacin, and mannopeptimycin. In general, the hydrophobic side chain is presumed to target the membrane to facilitate substrate binding and/or to disrupt (depolarize) the membrane. Increasing hydrophobic side-chain length increases the overall lipophilicity index of the drug and therefore is thought[9] to enhance membrane targeting. Specifically, for aryl-substituted disaccharide modified glycopeptides such as oritavancin, the drug hydrophobic side chain is thought[26] to target the bacterial membrane and enhance binding to lipid II. Although *in vitro* studies using lipid vesicles have shown that oritavancin is found at the membrane,[26] oritavancin and oritavancin-like glycopeptides are found as monomers *in vivo* bound to the peptidoglycan in the cell walls of intact whole-cells of *S. aureus* as discussed in the next section. It is therefore likely that any disruption of the membrane observed with

therapeutic-dosage levels is not caused by direct interaction of oritavancin-like glycopeptide side chains with the membrane.

Monomeric Binding and the $\Delta S/S_0$ Limit. FNCE binding to the peptidoglycan as a monomer is supported by the good agreement between the observed and estimated dephasing limits (Figures 7 and 8). Because there is only one ^{19}F−^{13}C distance observed for FNCE whole-cell cell-wall complexes (Figure 7, right), binding as a dimer would have reduced the asymptotic dephasing limit by a factor of 2 relative to the observed value. (Half the fluorines of the drug dimer would be out of dephasing range to the single nearest complexed D-[1-^{13}C]Ala of an uncross-linked stem; the same argument pertains to [^{19}F]oritavancin whole-cell complexes.) This places all FNCE bound within the cell wall. The lipophilic side chain of FNCE therefore cannot function as a membrane anchor. This conclusion is supported by the absence of ^{31}P{^{19}F} REDOR dephasing (Figure S4, left) for FNCE complexed to whole cells *S. aureus*, which places the ^{19}F away from the natural abundance ^{31}P of the lipid membrane. The side chain of [^{19}F]oritavancin is also not found within the membrane (Figure S4, right). In addition, as mentioned at the end of the Results, the absence of ^{13}C{^{19}F} dephasing of the lipid natural-abundance ^{13}C for FNCE and [^{19}F]oritavancin whole-cell complexes indicates no membrane insertion for either drug. Therefore, we conclude that both aryl and alkyl side chains of disaccharide-modified glycopeptides do not form specific membrane anchors. Because the chemical structure of FNCE closely resembles that of telavancin,[27] it is highly unlikely that the decylaminoethyl side chain of telavancin (Figure S2, top right) functions as a membrane anchor *in vivo* at therapeutic dosage levels.

Secondary Binding Site. We proposed before that the drug hydrophobic side chain is part of a secondary-binding site for disaccharide-modified glycopeptides.[10,14,28,29] This proposal was based on the observation that the position of ^{19}F in [^{19}F]oritavancin− and FPBV−peptidoglycan complexes is always found along the α-helix end of the pentaglycyl bridge near the cross-link. The pentaglycyl bridge segment in *S. aureus* appears to be encapsulated within the cleft formed by the aglycon and the drug side chain.[10,11,24] This cleft therefore is a secondary-binding site with the pentaglycyl bridge segment as the target. The drugs usually are found near the end of an uncross-linked pentapeptide stem.[29]

Side-Chain Length. The conformational analysis of [^{19}F]oritavancin− and FPBV−peptidoglycan complexes[10,11] showed that the side-chain lengths of 9 ECU resulted in more homogeneous binding and greater antimicrobial activity than for FBV with a side-chain length of 5 ECU.[14] The lengthening of the side chain to 13 ECU for *N*-(4-(4-biphenyl)benzyl)chloroeremomycin (Figure S1, bottom right) and FBBCE (Figure 1) results in reduced antimicrobial activity (Table S1). The conformational heterogeneity revealed for the FBBCE−peptidoglycan complex by the broad distribution for the distance from ^{19}F of FBBCE to ^{13}C of D-[1-^{13}C]alanine (Figure 3, right) suggests that the reduced activity is due to the loss of secondary binding resulting from a poor steric match between the long side chain and the pentaglycyl bridge. However, the best-fit ^{19}F position in the FBBCE−peptidoglycan complex is nearly identical to the best-fit ^{19}F position found in [^{19}F]oritavancin−peptidoglycan complexes. The ^{19}F position in FBBCE requires that the long terphenyl side chain tilt away from the pentaglycyl bridge segment, a steric mismatch that may account for reduced activity.

Rigid vs Flexible Side Chains. In FNCE, the rigid fluorophenylbenzyl side chain of [^{19}F]oritavancin is replaced by a highly flexible fluorononyl side chain. Both side chains have a length of 9 ECU. Despite the side-chain flexibility, the ^{19}F position in the FNCE–peptidoglycan complex is well-defined. A single ^{19}F–^{13}C distance of 8.0 Å (without a significant distribution) from the drug fluorine to the label of D-[1-^{13}C]alanine of the peptidoglycan stem (Figure 7, right) is consistent with homogeneous FNCE binding. The ^{19}F in the FNCE–peptidoglycan complex is found positioned along the α-helix end of the pentaglycyl bridge near the cross-link. The measured distance between ^{19}F to the nearest glycyl-carbonyl carbon is 7 Å, whereas this distance is 5 Å in the [^{19}F]oritavancin–peptidoglycan complex. Although the ^{19}F positions in FNCE– and [^{19}F]oritavancin–peptidoglycan complexes are not identical, the well-defined ^{19}F position of FNCE near the cross-link suggests that the pentaglycyl bridge segment is indeed encapsulated by the flexible fluorononyl side chain.

Summary of Binding Heterogeneity. The structural characterization of FBV–, LY309687–, and FBBCE–peptidoglycan complexes revealed that short (5–7 ECU) and long (13 ECU) rigid side chains contribute to conformational heterogeneity. In contrast, conformational homogeneity was observed for FPBV– and [^{19}F]oritavancin–peptidoglycan complexes, where the glycopeptides had side-chain lengths of 9 ECU (Figure 1).

Mode of Action. We have proposed a mode of action for disaccharide-modified glycopeptides[28,29] based on structural evidence that the drug side chain is part of a secondary-binding site. This site compensates for the loss of primary binding to the D-Ala-D-Lac terminated peptidoglycan found in VRE and VRSA, and explains the potent activities of Edman degradation products of oritavancin and oritavancin-like vancomycin, against both vancomycin-susceptible and -resistant bacteria.[7,28,30]

The secondary-binding site in oritavancin enables the drug to exhibit a unique dual mode of action in which both transglycosylase and transpeptidase activities of peptidoglycan biosynthesis in *S. aureus* are inhibited.[28] Oritavancin uses its D-Ala-D-Ala primary binding site to sequester lipid II just as vancomycin does.[31] In addition, oritavancin uses its secondary binding site to target partially cross-linked peptidoglycan. Oritavancin binding to the pentaglycyl-bridge segment of *nascent* peptidoglycan interferes with both the glycan chain-elongation by transglycosylase and incorporation of the nascent peptidoglycan to the surrounding cell wall by transpeptidase. Prevention of cell-wall maturation by oritavancin therefore disrupts the template-driven mechanism of peptidoglycan biosynthesis in Gram-positive bacteria.[14]

In summary, both aryl and alkyl side chains of disaccharide modified glycopeptides are involved in cell-wall binding by the formation of secondary-binding sites which target the pentaglycyl bridge segment of peptidoglycan in *S. aureus*. When this target is part of nascent peptidoglycan at the membrane surface, the bound drug actively interferes with peptidoglycan biosynthesis. The hydrophobic side chains in disaccharide-modified glycopeptides are not membrane anchors and do not mediate the formation of drug dimers in intact cells. Disaccharide-modified glycopeptides with a hydrophobic side-chain length of 9 ECU have the maximum activity by optimizing the steric matching between the drug side chain and the pentaglycyl bridge segment of peptidoglycan. We anticipate that all such glycopeptides will exhibit a dual mode of action similar to that of oritavancin.

■ ASSOCIATED CONTENT

Ⓢ Supporting Information

(i) Chemical structures of aryl side-chain containing chloroeremomycin derivatives; (ii) chemical structures of second generation semisynthetic lipoglycopeptides containing aromatic or aliphatic side chains; (iii) chemical syntheses of *N*-(4-(4-fluorobiphenyl)benzyl)chloroeremomycin (FBBCE) and *N*-(9-fluorononyl)chloroeremomycin (FNCE); (iv) minimum inhibitory concentrations (μg/mL) of fluorine-containing disaccharide-modified chloroeremomycins; (v) a brief general description of rotational-echo double-resonance NMR and the spectrometer used to obtain ^{31}P{^{19}F} REDOR spectra; and (vi) 202.4-MHz ^{31}P{^{19}F} REDOR spectra after 13.4 ms of dipolar evolution of FNCE and [^{19}F]oritavancin complexed to whole cells of *S. aureus*. This material is available free of charge via the Internet at http://pubs.acs.org.

■ AUTHOR INFORMATION

Corresponding Author
*Phone: 314-935-6844. Fax: 314-935-4481. E-mail: jschaefer@wustl.edu.

Notes
The authors declare no competing financial interest.

■ ACKNOWLEDGMENTS

■ ABBREVIATIONS USED

^{13}C{^{19}F}, carbon-channel observation with fluorine dephasing; ECU, equivalent carbon units; [^{19}F]oritavancin, *N*-(4-(4-fluorophenyl)benzyl)chloroeremomycin; FBBCE, *N*-(4-(4-fluorobiphenyl)benzyl)chloroeremomycin; FBV, *N*-(4-fluorobenzyl)vancomycin; FNCE, *N*-(9-fluorononyl)-chloroeremomycin; MAS, magic-angle spinning; MIC, minimum inhibitory concentration; ^{15}N{^{19}F}, nitrogen-channel observation with fluorine dephasing; ^{31}P{^{19}F}, phosphorus-channel observation with fluorine dephasing; REDOR, rotational-echo double resonance; VRE, vancomycin-resistant enterococci; VRSA, vancomycin-resistant *Staphylococcus aureus*

■ REFERENCES

(1) Rodriguez, M. J., Snyder, N. J., Zweifel, M. J., Wilkie, S. C., Stack, D. R., Cooper, R. D., Nicas, T. I., Mullen, D. L., Butler, T. F., and Thompson, R. C. (1998) Novel glycopeptide antibiotics: N-alkylated derivatives active against vancomycin-resistant enterococci. *J. Antibiot.* 51, 560−569.

(2) Cooper, R. D., Snyder, N. J., Zweifel, M. J., Staszak, M. A., Wilkie, S. C., Nicas, T. I., Mullen, D. L., Butler, T. F., Rodriguez, M. J., Huff, B. E., and Thompson, R. C. (1996) Reductive alkylation of glycopeptide antibiotics: synthesis and antibacterial activity. *J. Antibiot.* 49, 575−581.

(3) Arhin, F. F., Belley, A., McKay, G. A., and Moeck, G. (2010) Characterization of the in vitro activity of novel lipoglycopeptide antibiotics, in *Current Protocols in Microbiology*, Chapter 17, Unit 17.1, Wiley, New York.

(4) Vaudaux, P., Huggler, E., Arhin, F. F., Moeck, G., Renzoni, A., and Lew, D. P. (2009) Comparative activity of oritavancin against

meticillin-resistant *Staphylococcus aureus* (MRSA) bloodstream isolates from Geneva University Hospital. *Int. J. Antimicrob. Agents 34*, 540−543.

(5) Arhin, F. F., Sarmiento, I., Parr, T. R., Jr., and Moeck, G. (2009) Comparative in vitro activity of oritavancin against *Staphylococcus aureus* strains that are resistant, intermediate or heteroresistant to vancomycin. *J. Antimicrob. Chemother. 64*, 868−870.

(6) Beauregard, D. A., Williams, D. H., Gwynn, M. N., and Knowles, D. J. (1995) Dimerization and membrane anchors in extracellular targeting of vancomycin group antibiotics. *Antimicrob. Agents Chemother. 39*, 781−785.

(7) Ge, M., Chen, Z., Onishi, H. R., Kohler, J., Silver, L. L., Kerns, R., Fukuzawa, S., Thompson, C., and Kahne, D. (1999) Vancomycin derivatives that inhibit peptidoglycan biosynthesis without binding D-Ala-D-Ala. *Science 284*, 507−511.

(8) Sinha Roy, R., Yang, P., Kodali, S., Xiong, Y., Kim, R. M., Griffin, P. R., Onishi, H. R., Kohler, J., Silver, L. L., and Chapman, K. (2001) Direct interaction of a vancomycin derivative with bacterial enzymes involved in cell wall biosynthesis. *Chem. Biol. 8*, 1095−1106.

(9) Allen, N. E., LeTourneau, D. L., and Hobbs, J. N., Jr. (1997) The role of hydrophobic side chains as determinants of antibacterial activity of semisynthetic glycopeptide antibiotics. *J. Antibiot. 50*, 677−684.

(10) Kim, S. J., Cegelski, L., Studelska, D. R., O'Connor, R. D., Mehta, A. K., and Schaefer, J. (2002) Rotational-echo double resonance characterization of vancomycin binding sites in *Staphylococcus aureus*. *Biochemistry 41*, 6967−6977.

(11) Kim, S. J., Cegelski, L., Preobrazhenskaya, M., and Schaefer, J. (2006) Structures of *Staphylococcus aureus* cell-wall complexes with vancomycin, eremomycin, and chloroeremomycin derivatives by ^{13}C-$\{^{19}$F$\}$ and ^{15}N$\{^{19}$F$\}$ rotational-echo double resonance. *Biochemistry 45*, 5235−5250.

(12) Kim, S. J., Singh, M., and Schaefer, J. (2009) Oritavancin binds to isolated protoplast membranes but not intact protoplasts of *Staphylococcus aureus*. *J. Mol. Biol. 391*, 414−425.

(13) Patti, G. J., Kim, S. J., Yu, T. Y., Dietrich, E., Tanaka, K. S., Parr, T. R., Jr., Far, A. R., and Schaefer, J. (2009) Vancomycin and oritavancin have different modes of action in *Enterococcus faecium*. *J. Mol. Biol. 392*, 1178−1191.

(14) Kim, S. J., and Schaefer, J. (2008) Hydrophobic side-chain length determines activity and conformational heterogeneity of a vancomycin derivative bound to the cell wall of *Staphylococcus aureus*. *Biochemistry 47*, 10155−10161.

(15) Gullion, T., and Schaefer, J. (1989) Detection of weak heteronuclear dipolar coupling by rotational-echo double-resonance nuclear magnetic resonance. *Adv. Magn. Reson. 13*, 57−83.

(16) Tong, G., Pan, Y., Dong, H., Pryor, R., Wilson, G. E., and Schaefer, J. (1997) Structure and dynamics of pentaglycyl bridges in the cell walls of *Staphylococcus aureus* by ^{13}C-^{15}N REDOR NMR. *Biochemistry 36*, 9859−9866.

(17) Bennett, A. E., Reienstra, C. M., Auger, M., Lakshmi, K. V., and Griffin, R. G. (1995) Heteronuclear decoupling in rotating solids. *J. Chem. Phys. 103*, 6951−6958.

(18) Stueber, D., Mehta, A. K., Chen, Z., Wooley, K. L., and Schaefer, J. (2006) Local order in polycarbonate glasses by ^{13}C$\{^{19}$F$\}$ Rotational-Echo Double-Resonance NMR. *J. Polym. Sci., Part B: Polym. Phys. 44*, 2760−2775.

(19) Gullion, T., Baker, D. B., and Conradi, M. S. (1990) New, compensated Carr-Purcell sequences. *J. Magn. Reson. 89*, 479−484.

(20) Weldeghiorghis, T. K., and Schaefer, J. (2003) Compensating for pulse imperfections in REDOR. *J. Magn. Reson. 165*, 230−236.

(21) Mueller, K. T., Jarvie, T. P., Aurentz, D. J., and Roberts, B. W. (1995) The REDOR transform: direct calculation of internuclear couplings from dipolar-dephasing NMR data. *Chem. Phys. Lett. 242*, 535−542.

(22) de la Caillerie, J.-B. d. E., and Fretigny, C. (1998) Analysis of the REDOR signal and inversion. *J. Magn. Reson. 133*, 273−280.

(23) O'Connor, R. D., and Schaefer, J. (2002) Relative CSA-dipolar orientation from REDOR sidebands. *J. Magn. Reson. 154*, 46−52.

(24) Cegelski, L., Steuber, D., Mehta, A. K., Kulp, D. W., Axelsen, P. H., and Schaefer, J. (2006) Conformational and quantitative characterization of oritavancin-peptidoglycan complexes in whole cells of *Staphylococcus aureus* by in vivo ^{13}C and ^{15}N labeling. *J. Mol. Biol. 357*, 1253−1262.

(25) Toke, O., Maloy, W. L., Kim, S. J., Blazyk, J., and Schaefer, J. (2004) Secondary Structure and Lipid Contact of a Peptide Antibiotic in Phospholipid Bilayers by REDOR. *Biophys. J. 87*, 662−674.

(26) Domenech, O., Francius, G., Tulkens, P. M., Van Bambeke, F., Dufrene, Y., and Mingeot-Leclercq, M. P. (2009) Interactions of oritavancin, a new lipoglycopeptide derived from vancomycin, with phospholipid bilayers: Effect on membrane permeability and nanoscale lipid membrane organization. *Biochim. Biophys. Acta 1788*, 1832−1840.

(27) Lunde, C. S., Hartouni, S. R., Janc, J. W., Mammen, M., Humphrey, P. P., and Benton, B. M. (2009) Telavancin disrupts the functional integrity of the bacterial membrane through targeted interaction with the cell wall precursor lipid II. *Antimicrob. Agents Chemother. 53*, 3375−3383.

(28) Kim, S. J., Cegelski, L., Stueber, D., Singh, M., Dietrich, E., Tanaka, K. S., Parr, T. R., Far, A. R., and Schaefer, J. (2008) Oritavancin exhibits dual mode of action to inhibit cell-wall biosynthesis in *Staphylococcus aureus*. *J. Mol. Biol. 377*, 281−293.

(29) Kim, S. J., Matsuoka, S., Patti, G. J., and Schaefer, J. (2008) Vancomycin derivative with damaged D-Ala-D-Ala binding cleft binds to cross-linked peptidoglycan in the cell wall of *Staphylococcus aureus*. *Biochemistry 47*, 3822−3831.

(30) Goldman, R. C., Baizman, E. R., Longley, C. B., and Branstrom, A. A. (2000) Chlorobiphenyl-desleucyl-vancomycin inhibits the transglycosylation process required for peptidoglycan synthesis in bacteria in the absence of dipeptide binding. *FEMS Microbiol. Lett. 183*, 209−214.

(31) Cegelski, L., Kim, S. J., Hing, A. W., Studelska, D. R., O'Connor, R. D., Mehta, A. K., and Schaefer, J. (2002) Rotational-echo double resonance characterization of the effects of vancomycin on cell wall synthesis in *Staphylococcus aureus*. *Biochemistry 41*, 13053−13058.